Condensation, demixing, and orientational ordering of magnetic colloidal suspensions

Stefanie M. Cattes,[1] Sabine H. L. Klapp,[2] and Martin Schoen[1,3]

[1]*Stranski-Laboratorium für Physikalische und Theoretische Chemie, Fakultät für Mathematik und Naturwissenschaften, Technische Universität Berlin, Straße des 17. Juni 115, 10623 Berlin, Germany*

[2]*Institut für Theoretische Physik, Fakultät für Mathematik und Naturwissenschaften, Technische Universität Berlin, Hardenbergstr. 36, 10623 Berlin, Germany*

[3]*Department of Chemical and Biomolecular Engineering, Engineering Building I, Box 7905, North Carolina State University, 911 Partners Way, Raleigh, North Carolina 27695, USA*

(Received 5 February 2015; published 15 May 2015)

In this work we study the phase behavior of magnetic particles suspended in a simple nonmagnetic solvent. Magnetic particles are modelled as spherical particles carrying a three-dimensional, classical Heisenberg spin, whereas solvent molecules are treated as spherically symmetric Lennard-Jones particles. The binary mixture of magnetic particles and solvent is studied within the framework of classical density functional theory (DFT). Within DFT pair correlations are treated at the modified mean-field level at which they are approximated by orientation dependent Mayer f functions. In the absence of an external magnetic field four generic types of phase diagrams are observed depending on the concentration of magnetic particles. In this case we observe liquid-liquid phase coexistence between an orientationally ordered (polarized) and a disordered phase characterized by slightly different concentrations of magnetic particles. Liquid-liquid phase coexistence is suppressed by an external field and vanishes completely if the strength of the field is sufficiently large.

DOI: 10.1103/PhysRevE.91.052127 PACS number(s): 05.20.Jj, 64.60.A−, 64.60.fd

I. INTRODUCTION

Understanding the phase behavior of (model) fluids consisting of spherical particles with an internal, vectorial degree of freedom by theory and computer simulations has attracted attention for decades and still continues to do so [1,2]. Prominent examples of such systems are "spin" fluids where the spheres carry a discrete, one-dimensional (1D) [3], a continuous XY (2D) [2,4], or a classical Heisenberg (3D) spin [5–9].

These models have been originally introduced as classical off-lattice counterparts of corresponding (quantum) models for magnetic solids and have thus raised fundamental interest in their own right [1,2]. From a physical point of view, the XY fluid is often considered as a candidate to describe superfluid transitions in pure ^{4}He [2,10], whereas the Heisenberg fluid serves as the most basic model to describe *magnetic* ordering in fluids [5–9], particularly in undercooled liquid alloys. Moreover, Heisenberg-like interactions also occur in models of amphiphilic colloidal spheres with an internal anisotropy stemming from two different materials (so-called Janus particles) [11–13]. Further important and well-studied examples of spherical, anisotropic particles are dipolar (hard or soft) spheres (see, e.g., Refs. [14–17]), where the spin is replaced by a point dipole moment yielding a model ferrocolloid, and variants of these describing more complex (e.g., capped) magnetic particles [18,19]. Typical methods of investigation targeting the phase behavior include Monte Carlo (MC) or molecular dynamics computer simulations [5,8,13–15], classical density functional theory (DFT) involving (approximate) free-energy functionals [8,16,20], and integral equation approaches [2,5,6,17].

Many, yet not all, of these studies focused on the one-component case, either without or in the presence of an external ordering field. These systems already show rich phase behavior characterized by gas-liquid transitions and transitions into orientationally ordered phases, accompanied by tricritical, critical end, and triple points (see, e.g., Ref. [2] and references therein). However, more recently also (binary) *mixtures* involving anisotropic spheres have been studied, such as Ising mixtures [21], mixtures of dipolar spheres characterized by different dipolar coupling strengths [22–26], as well as mixtures of dipolar and neutral spheres [22,27–29]. In general, phase separation in mixtures is relevant, for example, to evaluate the stability of molecular and colloidal solutions [30] and to understand the interactions between nanoparticles and macromolecules including novel phenomena such as Casimir forces [31]. Moreover, knowledge of the bulk phase behavior of a mixture is crucial to understand interfacial and confinement effects occurring in the presence of surfaces. Such effects can be particularly pronounced in mixtures involving internal degrees of freedom and a resulting sensitivity to an external field. For example, recent MC simulations of a mixture of dipolar and hard spheres under confinement [28] have reported a field-induced inversion of the composition in the (slitlike) pore, and related instabilities are seen close to an electrode [27]. Finally, an issue gaining increasing attention is the theoretical description of colloidal mixtures in *nonequilibrium*, e.g., in the context of spinodal decomposition [32–34], in the presence of sedimentation [35] or due to a time-dependent field. Again, internal degrees of freedom here lead to a variety of new behaviors. An example is the symmetry-breaking pattern formation of a two-dimensional, phase-separating magnetic mixture in a magnetic ratchet field [36]. Clearly, a precise understanding of such nonequilibrium phenomena has as its foundation knowledge of the equilibrium phase diagram.

Motivated by these issues we present here an equilibrium DFT of the phase behavior of a three-dimensional, binary fluid composed of Heisenberg particles carrying a magnetic (3D) spin and simple spheres. Both zero-field systems and the case of an external field are considered. The Heisenberg mixture can be viewed as the most basic model for a

colloidal suspension including both magnetic particles and nonmagnetic particles such as polymers. Such mixtures are promising candidates for the controlled fabrication of patterns on the micron scale [37]. Following previous work on Janus fluids [12,13] and one-component Heisenberg fluids [8], our DFT approach invokes the so-called modified mean field (MMF) approximation [38] involving a Boltzmann *ansatz* for the two-particle correlation functions.

We deliberately consider mixtures with Heisenberg particles rather than the more complicated case of dipolar mixtures for the following reasons. First, extensive density functional studies of dipolar mixtures already exist [25,26], whereas the simpler case of a Heisenberg mixture has, to our knowledge, only been studied in two dimensions [33,34] and for a limited set of parameters. Thus, the global phase behavior in three dimensions is not known. This somehow contrasts the importance of the model not only for magnetic-nonmagnetic mixtures but also for other complex colloids such as mixtures involving Janus spheres [12,13].

Second, previous studies of one-component Heisenberg fluids [8] and related systems [12,13] have demonstrated that a reasonable free-energy approximation such as the MMF-DFT yield predictions for the ferromagnetic transitions which are in *semiquantitative* agreement with corresponding MC results. This differs in dipolar systems where the long-range directional dependence (resulting from the coupling of distance and orientation vectors) of the pair interactions implies profound challenges for theoretical descriptions. Indeed, many specific consequences of dipolar interactions such as aggregation at low densities (see, for example, Ref. [15] for a recent discussion) and the competition between ordering and frustration at high densities (see, for example, Refs. [14,39]) are still beyond the capabilities of standard DFT (and integral-equation) methods.

As an example in the mixture case, recent MC simulations of dipolar-hard sphere mixtures have shown [29] that the theoretically predicted demixing transition temperatures are significantly overestimated. For the (ferromagnetic) off-lattice Heisenberg system, on the other hand, the interaction is not only of short range (as modelled, e.g., by a Yukawa- or van-der Waals-like potential) but also *separable*; therefore frustration does not exist. This leads to a much better performance of mean-field-like DFT approaches for one-component Heisenberg fluids [5,8,13], and a similar accuracy can be expected for mixtures. Having this in mind, the overall goal of our density functional study is to predict the morphologies of all possible phase diagrams in the fluid regime.

The remainder of this paper is organized as follows. In Sec. II we introduce the model potential for our Heisenberg mixture and Sec. III summarizes key elements of the DFT theory on which our theoretical work is based. Numerical results for various mixtures without and in presence of an external field are presented in Sec. IV. The paper concludes with a summary of our main findings in Sec. V.

II. MODEL SYSTEM

A. Isotropic interactions

We consider a binary fluid mixture consisting of spherically symmetric solvent molecules (component 1) and spherical nanoparticles carrying a classical, three-dimensional (Heisenberg) spin. Particles of both species have a hard core of the same diameter σ such that the interaction between these cores is described by the hard-sphere potential function

$$\varphi_{\rm hs}(r_{12}) = \begin{cases} \infty, & r_{12} < \sigma \\ 0, & r_{12} \geqslant \sigma \end{cases}, \tag{2.1}$$

irrespective of the components to which the interacting molecules pertain. In Eq. (2.1), $r_{12} = |\boldsymbol{r}_{12}| = |\boldsymbol{r}_1 - \boldsymbol{r}_2|$ is the distance between the centers of the hard cores located at $\boldsymbol{r}_1$ and $\boldsymbol{r}_2$, respectively.

For distances $r_{12} \geqslant \sigma$, a (generally) anisotropic attraction is superimposed to the hard-sphere repulsion. It can be cast as

$$\varphi_{ab}(\boldsymbol{r}_{12},\omega_1,\omega_2) = \varphi_{ab}^{\rm iso}(r_{12}) + \varphi_{\rm anis}(\boldsymbol{r}_{12},\omega_1,\omega_2)\,\delta_{a2}\delta_{b2}, \tag{2.2}$$

where $a,b = 1,2$ labels the mixture component and the δ's denote Kronecker symbols.

In Eq. (2.2), $\omega_i = (\theta_i,\phi_i)$ $(i = 1,2)$, where θ_i and ϕ_i are Euler angles specifying the orientation of uniaxial molecules in a space-fixed frame of reference. In writing Eq. (2.2) we assume orientation-dependent interactions ($\varphi_{\rm anis}$) only within component 2. Focusing exclusively on dispersion interactions we take $\varphi_{ab}^{\rm iso}$ to be given by the well-known Lennard-Jones potential, that is,

$$\varphi_{ab}^{\rm iso}(r_{12}) = 4\varepsilon_{ab}\left[\left(\frac{\sigma}{r_{12}}\right)^{12} - \left(\frac{\sigma}{r_{12}}\right)^{6}\right], \tag{2.3}$$

where ε_{ab} is the depth of the attractive well associated with the interaction between molecules of components a and b. To limit the dimensions of the parameter space of our model we shall be concerned exclusively with so-called pseudomixtures for which in general $\varepsilon_{11} = \varepsilon_{22} \equiv \varepsilon \neq \varepsilon_{12}$.

B. Anisotropic attractions

To describe the interaction between a pair of (Heisenberg) spins we adopt

$$\begin{aligned}\varphi_{\rm anis}(\boldsymbol{r}_{12},\omega_1,\omega_2) &= -4\varepsilon\varepsilon_H\left(\frac{\sigma}{r_{12}}\right)^6 \widehat{\mathbf{u}}(\omega_1)\cdot\widehat{\mathbf{u}}(\omega_2) \\ &= \frac{4(4\pi)^{3/2}}{\sqrt{3}}\varepsilon\varepsilon_H\left(\frac{\sigma}{r_{12}}\right)^6 \Phi_{110}(\omega_1,\omega_2,\omega),\end{aligned} \tag{2.4}$$

where $\widehat{\boldsymbol{u}}(\omega_i)$ $(i = 1,2)$ is a unit vector specifying the orientation of molecule i of component 2. The dimensionless parameter ε_H introduced in Eq. (2.4) permits us to control the coupling strength between a pair of interacting spins. Here we assume $\varepsilon_H \geqslant 0$ corresponding to ferromagnetic coupling. In Eq. (2.4), ω specifies the orientation of $\widehat{\boldsymbol{r}}_{12} = \boldsymbol{r}_{12}/r_{12}$.

The quantity Φ_{110} in Eq. (2.4) is a rotational invariant [13,40] which can be cast more explicitly as

$$\begin{aligned}\Phi_{110}(\omega_1,\omega_2,\omega) &= -\frac{1}{(4\pi)^{3/2}}\frac{1}{\sqrt{3}}[\mathcal{Y}_{11}^*(\omega_1)\,\mathcal{Y}_{11}(\omega_2) \\ &\quad + \mathcal{Y}_{11}(\omega_1)\,\mathcal{Y}_{11}^*(\omega_2) + \mathcal{Y}_{10}(\omega_1)\,\mathcal{Y}_{10}(\omega_2)] \\ &= \widehat{\boldsymbol{u}}(\omega_1)\cdot\widehat{\boldsymbol{u}}(\omega_2).\end{aligned} \tag{2.5}$$

In Eq. (2.5), $\mathcal{Y}_{lm}$ is a spherical harmonic and the asterisk denotes the complex conjugate [40].

In addition to the intermolecular interactions we allow for the presence of a homogeneous (i.e., nonlocal) external field $\boldsymbol{H}$ capable of interacting with the spins of the magnetic particles. Hence, we have a one-body external potential,

$$\varphi_{\text{ext}}(\omega_2) = -\boldsymbol{H}\cdot\widehat{\boldsymbol{u}}(\omega_2) = -H\cos\theta_2 = -H P_1(x), \quad (2.6)$$

where $x \equiv \cos\theta_2$ and P_1 is the first Legendre polynomial. In writing Eq. (2.6) we assumed without loss of generality that the external field, if present, points along the z axis of our space-fixed frame of reference and $H = |\boldsymbol{H}|$ is the magnitude of the external field.

III. ELEMENTS OF DENSITY FUNCTIONAL THEORY

A. Modified mean-field grand-potential functional

In this work we employ classical DFT to study the phase behavior of the model introduced in Sec. II. Hence, we are seeking minima of the grand potential functional

$$\Omega[\{\rho_a(\boldsymbol{r},\omega)\}] = \mathcal{F}[\{\rho_a(\boldsymbol{r},\omega)\}] - \sum_a \mu_a \int d\boldsymbol{r}\, d\omega\, \rho_a(\boldsymbol{r},\omega), \quad (3.1)$$

where $\mathcal{F}$ is the free-energy functional, μ_a is the chemical potential of component a, and $\rho_a(\boldsymbol{r},\omega)$ is the orientation-dependent, singlet density of that mixture compound. The free-energy functional can be written as a sum of five terms,

$$\mathcal{F} = \mathcal{F}_{\text{id}} + \mathcal{F}_{\text{or}} + \mathcal{F}_{\text{ext}} + \mathcal{F}_{\text{hs}} + \Delta\mathcal{F}_{\text{ex}}, \quad (3.2)$$

where we have dropped the arguments to ease the notational burden.

In Eq. (3.2) the last two terms correspond to the interaction (excess) part of the free energy. Specifically, $\mathcal{F}_{\text{hs}}$ is the contribution from the hard-sphere reference system [see Eq. (3.14)] and $\Delta\mathcal{F}_{\text{ex}}$ corresponds to the change in free energy between the single-component hard-sphere reference system and the fully interacting binary mixture [see Eqs. (2.1) and (2.2)]. Within the so-called MMF approximation [12,22,38,41,42], where one approximates the pair correlation functions via

$$g_{ab}(\boldsymbol{r}_{12},\omega_1,\omega_2) = \begin{cases} 0, & r_{12} < \sigma \\ \exp\left[-\beta\left(\varphi_{\text{hs}} + \varphi_{ab}\right)\right], & r_{12} \geqslant \sigma, \end{cases} \quad (3.3)$$

it is straightforward to show that [12]

$$\beta\Delta\mathcal{F}_{\text{ex}} = -\frac{1}{2}\sum_{a,b}\int_{r_{12}\geqslant\sigma} d\boldsymbol{r}_1\, d\boldsymbol{r}_2 \int d\omega_1\, d\omega_2\, \rho_a(\boldsymbol{r}_1,\omega_1) \times \rho_b(\boldsymbol{r}_2,\omega_2)\, f_{ab}(\boldsymbol{r}_{12},\omega_1,\omega_2), \quad (3.4)$$

where $\beta \equiv 1/k_B T$ (k_B is Boltzmann's constant and T is temperature). In Eq. (3.4), the quantity $f_{ab} \equiv \exp(-\beta\varphi_{ab}) - 1$ is the Mayer f function for the interaction between a molecular pair of components a and b. Notice that in the limit of vanishing density Eq. (3.3) becomes exact.

Because we are interested in binary fluid mixtures without any positional order we may describe the singlet densities in Eq. (3.4) by

$$\rho_1(\boldsymbol{r},\omega) = \frac{\rho_1}{4\pi}, \quad (3.5)$$

$$\rho_2(\boldsymbol{r},\omega) = \rho_2\alpha(\omega), \quad (3.6)$$

where ρ_a is the partial number density of component a and $\alpha(\omega)$ is the orientation distribution function normalized according to

$$\int d\omega\, \alpha(\omega) = 1. \quad (3.7)$$

We note in passing that Eqs. (3.5) and (3.6) remain valid for $H \neq 0$ on account of the nonlocality of $\boldsymbol{H}$. Because only the magnetic particles (component 2) carry a spin, the Mayer f functions f_{11} and f_{12} depend only on r_{12} such that the integration over orientations in Eq. (3.4) can be carried out trivially using Eq. (3.7) and the fact that $\int d\omega = 4\pi$. For f_{22} [see Eq. (2.2)] the resulting free-energy contributions can be derived as detailed elsewhere [12]. Hence, we eventually arrive at

$$\frac{\beta\Delta\mathcal{F}_{\text{ex}}}{V} = \frac{1}{4}\sum_{a,b}\rho_a\rho_b u_0^{(ab)} + \rho_2^2\sum_{l=1}^{\infty}\alpha_l^2 u_l^{(22)}. \quad (3.8)$$

In Eq. (3.8), V denotes volume,

$$u_l^{(ab)} = -\frac{(-1)^l}{\sqrt{\pi}\,(2l+1)^{3/2}}\int_\sigma^\infty dr_{12}\, r_{12}^2\, f_{ll0}^{(ab)}(r_{12}) \quad (3.9)$$

accounts for the contribution of attractive interactions arising for $r_{12} \geqslant \sigma$ between particles of both species, and the coefficients $f_{ll0}^{(ab)}$ are obtained from an expansion of the corresponding f_{ab} in the basis of rotational invariants [13]. In Eq. (3.9), the expression for $l = 0$ is related to the isotropic contribution to φ_{ab}. Because of our choice $\varepsilon_{11} = \varepsilon_{22} = \varepsilon$, $u_0^{(11)} = u_0^{(22)} = u_0$ and we shall retain the superscript only for $u_0^{(12)}$ which differs in general from u_0 because $\varepsilon \neq \varepsilon_{12}$ in binary pseudomixtures. Moreover, because only the interaction between a pair of magnetic particles contributes to the second term on the right-hand side of Eq. (3.8), we shall also drop the superscript on $u_l^{(22)}$ for $l \geqslant 1$ henceforth.

Members of the set $\{\alpha_l\}$ in Eq. (3.8) are coefficients introduced through the expansion of the orientation distribution function

$$2\pi\alpha(\omega) = \overline{\alpha}(x) = \frac{1}{2} + \sum_{l=1}^{\infty}\alpha_l P_l(x) \quad (3.10)$$

in terms of Legendre polynomials P_l. This expansion is adequate here because of the uniaxial symmetry of ordered phases. In this expression, $\alpha_0 = \frac{1}{2}$ is treated separately because it arises regardless of whether one of the components of the mixture is orientationally ordered. Notice that the uniaxial symmetry of ordered phases is preserved even in the case $H \neq 0$. Because of the orthogonality of Legendre polynomials (see Eq. (A.9b) of Ref. [40]) we introduce order parameters

$$\mathcal{P}_l \equiv \frac{2}{2l+1}\alpha_l = \int_{-1}^{1} dx\, \overline{\alpha}(x)\, P_l(x), \qquad l \geqslant 1, \quad (3.11)$$

to quantify the order in different phases. In disordered phases these order parameters vanish, whereas in ordered phases they are nonzero regardless of l.

The presence of the external field also causes a contribution to the mixture's free energy that may be cast as

$$\begin{aligned}\frac{\beta\mathcal{F}_{\rm ext}}{V} &= -H\int d\boldsymbol{r}\, d\omega\, \rho_2(\boldsymbol{r},\omega)\,\varphi_{\rm ext}(\omega)\\ &= -\beta H\rho_2\int dx\,\overline{\alpha}(x)\,P_1(x)\\ &= -\beta H\rho_2\mathcal{P}_1,\end{aligned}\tag{3.12}$$

where the bottom line follows from Eqs. (2.6), (3.6), and (3.11).

Associated with the formation of ordered phases in the presence or absence of the external field, a loss of orientational entropy needs to be accounted for when such an orderd phase forms. Because this entropic loss affects only the magnetic particles the corresponding free-energy contribution may be expressed as

$$\frac{\beta\mathcal{F}_{\rm or}}{V} = \rho_2\int dx\,\overline{\alpha}(x)\,\ln\left[2\overline{\alpha}(x)\right],\tag{3.13}$$

which has the same functional form as in the case of a pure fluid composed of only the magnetic particles [13].

For the hard-sphere contribution to the free-energy functional we adopt the well-known Carnahan-Starling expression [43]

$$\frac{\beta\mathcal{F}_{\rm hs}}{V}\equiv\beta f_{\rm hs}=\rho\frac{4\eta-3\eta^2}{(1-\eta)^2},\tag{3.14}$$

which is valid here because we are assuming the hard spheres of both components to be of equal diameter [22]. In Eq. (3.14), $\rho=\rho_1+\rho_2$ is the total number density and $\eta=\frac{\pi}{6}\rho\sigma^3$ is the total hard-sphere packing fraction.

Finally, the ideal-gas contribution can be expressed as

$$\frac{\beta\mathcal{F}_{\rm id}}{V}=\rho_1[\ln(\rho_1\Lambda^3)-1]+\rho_2[\ln(\rho_2\Lambda^5 m/\mathcal{I})-1],\tag{3.15}$$

where $\Lambda=\sqrt{\beta h^2/2\pi m}$ is the thermal de Broglie wavelength, h denotes Planck's constant, m is the particle mass (which we assume to be the same for both components), and $\mathcal{I}$ is the moment of inertia of a uniaxial magnetic particle. Because we will eventually be dealing with mixtures at equilibrium, specific values for Λ, m, and $\mathcal{I}$ are irrelevant. This is reflected by the fact that these quantities do not appear in the final equations as one can see from Eqs. (A1)–(A3). These three equations are forming a subset of the nonlinear equations that we need to solve numerically in our search for coexisting phases at thermodynamic equilibrium.

B. Equilibrium states and phase coexistence

Focusing on these equilibrium states, the equations

$$\frac{\beta}{V}\left(\frac{\partial\Omega}{\partial\rho_1}\right)_{T,V}=0,\tag{3.16}$$

$$\frac{\beta}{V}\left(\frac{\partial\Omega}{\partial\rho_2}\right)_{T,V}=0,\tag{3.17}$$

$$\frac{\beta}{V}\frac{\delta\Omega}{\delta\overline{\alpha}(x)}=\lambda(T,\rho_2),\tag{3.18}$$

need to be satisfied simultaneneously, where λ is a Lagrangian multiplier. It serves to guarantee that any solution of Eq. (3.18) is always properly normalized [see Eq. (3.7)] and the δ operator in Eq. (3.18) indicates a functional derivative.

It is then straightforward to show that Eq. (3.16) can be recast as

$$0=\ln(\rho_1\Lambda^3)+\beta\mu_{\rm hs}+\tfrac{1}{2}\left(\rho_1 u_0+\rho_2 u_0^{(12)}\right)-\beta\mu_1,\tag{3.19}$$

where $\mu_{\rm hs}=(\partial f_{\rm hs}/\partial\rho)_{T,V}$ is the chemical potential of the hard-sphere reference fluid. Likewise, we obtain from Eq. (3.17) the expression

$$\begin{aligned}0=\ln(\rho_2\Lambda^5 m/\mathcal{I})+\int_{-1}^{1}dx\,\overline{\alpha}(x)\,\ln\left[2\overline{\alpha}(x)\right]-\frac{2}{3}\beta H\alpha_1\\ +\beta\mu_{\rm hs}+\frac{1}{2}\left(\rho_1 u_0^{(12)}+\rho_2 u_0\right)+2\rho_2\sum_{l=1}^{\infty}u_l\alpha_l^2-\beta\mu_2.\end{aligned}\tag{3.20}$$

As for pure fluids composed of magnetic particles [8,13] we also have

$$\begin{aligned}\int_{-1}^{1}dx\,\overline{\alpha}(x)\ln\left[2\overline{\alpha}(x)\right]=\frac{u_0}{2}\rho_2-\ln\frac{1}{2}\int_{-1}^{1}dx\,\Psi(x;H)\\ -2\rho_2\sum_{l=0}^{\infty}u_l\alpha_l^2,\end{aligned}\tag{3.21}$$

which satisfies Eq. (3.18). In Eq. (3.21),

$$\Psi(x;H)\equiv\exp\left[-\rho_2\sum_{l=1}^{\infty}(2l+1)\,u_l\alpha_l P_l(x)+\beta H P_1(x)\right].\tag{3.22}$$

Thus, combining Eqs. (3.20) and (3.21) allows us to introduce the expression

$$\begin{aligned}0=\ln(\rho_2\Lambda^5 m/\mathcal{I})-\ln\frac{1}{2}\int_{-1}^{1}dx\,\Psi(x;H)-\beta H\mathcal{P}_1\\ +\beta\mu_{\rm hs}+\frac{1}{2}\left(\rho_1 u_0^{(12)}+\rho_2 u_0\right)-\beta\mu_2.\end{aligned}\tag{3.23}$$

Next, to obtain a closed expression for the grand potential for a globally stable or metastable equilibrium state we solve Eqs. (3.19) and (3.23) for $\beta\mu_1$ and $\beta\mu_2$, respectively, and replace the corresponding terms in Eq. (3.1). Using also Eqs. (3.2), (3.8), and (3.12)–(3.15) it is straightforward to demonstrate that

$$\begin{aligned}\frac{\beta\Omega}{V}=-\beta P=-\rho+\beta f_{\rm fs}+\beta\rho\mu_{\rm hs}+\frac{u_0}{4}\left(\rho_1^2+\rho_2^2\right)\\ +\frac{u_0^{(12)}}{2}\rho_1\rho_2-\rho_2^2\sum_{l=1}^{\infty}u_l\alpha_l^2,\end{aligned}\tag{3.24}$$

where P denotes pressure.

A number of comments seem appropriate at this stage. First, Eq. (3.24) no longer depends on Λ, m, or $\mathcal{I}$, which is to be expected because Eq. (3.24) explicitly assumes equilibrium conditions. Second, $\lim_{\rho_1,\rho_2\to 0}\beta\Omega/V=-\rho$ and thus reduces to the ideal-gas limit as it must. This is because, except for the first term on the right-hand side of Eq. (3.24), all

other terms depend on the partial number densities at least quadratically in leading order. Third, Eq. (3.24) does not depend *explicitly* on the external field H which enters this equation only *implicitly* via $\{\mathcal{P}_l\}$. The latter becomes apparent by realizing that Eq. (3.11) can be recast as [12]

$$\mathcal{P}_l = \frac{\int_{-1}^{1} dx\, \Psi(x;H)\, P_l(x)}{\int_{-1}^{1} dx\, \Psi(x;H)}. \tag{3.25}$$

IV. RESULTS

A. Numerical details

In the following we express all physical quantities in dimensionless (i.e., "reduced") units. For example, energy is given in units of ε [see Eq. (2.3)] and length is given in terms of the hard-sphere diameter σ [see Eq. (2.1)]. Other quantities are given in terms of suitable combinations of these basic parameters. For example, T is expressed in units of ε/k_B, density in units of σ^{-3}, pressure in units of ε/σ^3, and the external field is given in units of ε.

To determine the phase diagram between pairs of phases labeled $'$ and $''$ we need to solve a system of six nonlinear coupled equations for the variables ρ_1', ρ_2', $\mathcal{P}_1'$, ρ_1'', ρ_2'', and $\mathcal{P}_1''$. As in our previous work [13] we truncate the expansion on the right-hand side of Eq. (3.22) after the leading term proportional to $l = 1$. Therefore, $\mathcal{P}_1$ is the only order parameter to be considered.

As we showed in Sec. III B, coexisting phases at thermodynamic equilibrium are characterized by values of ρ_1', ρ_2', $\mathcal{P}_1'$, ρ_1'', ρ_2'', and $\mathcal{P}_1''$ satisfying Eqs. (3.20) and (3.23)–(3.25). These values can be obtained by solving the coupled set of Eqs. (A1)–(A5) simultaneously, which we accomplish iteratively by a simple Newton-Raphson scheme (see also Appendix or Ref. [13]). More specifically, we need to solve the pair of equations

$$\boldsymbol{s}(\boldsymbol{x}^{(n)}) = -\mathbf{J}(\boldsymbol{x}^{(n)}) \cdot \delta\boldsymbol{x}^{(n)}, \tag{4.1}$$

$$\boldsymbol{x}^{(n+1)} = \boldsymbol{x}^{(n)} + \delta\boldsymbol{x}^{(n)}, \tag{4.2}$$

in vector notation where elements s_i of $\boldsymbol{s}$ are the six functions introduced in Eqs. (A1)–(A5), elements of the vector $\boldsymbol{x}^{(n)}$ are given by the actual values of the six variables ρ_1', ρ_2', α_1', ρ_1'', ρ_2'', and α_1'' in the n-th iteration, and the vector $\delta\boldsymbol{x}^{(n)}$ is a (sufficiently small) correction to these values that allows us to compute improved guesses for the six variables in the $(n+1)$-th iteration. The iteration is halted if $\max\left|\delta\boldsymbol{x}^{(n)}\right| \leqslant 10^{-6}$. Within the framework of the Newton-Raphson scheme, the Jacobian $\mathbf{J}$ is a 6×6 matrix whose elements are partial derivatives of $\boldsymbol{s}$ with respect to elements of $\boldsymbol{x}$. Because of the simplicity with which $\mathbf{J}$ can be derived no explicit expressions are given here.

Thermodynamic states at coexistence depend on T, H, and the concentration of magnetic particles in the higher-density (ordered or disordered) phase denoted as x_2'' for given model parameters ε_H and ε_{12}. Notice that for nonzero H the gas phase may also be ordered to some extent such that $\mathcal{P}_1' \neq 0$ in general; $\mathcal{P}_1' = 0$ only for the special case $H = 0$ regardless of T and x_2''.

The standard temperature increment for which phase diagrams below have been generated is $\Delta T = 10^{-4}$. Based upon that, resolution lines are plotted in the phase diagrams shown below. To enhance the clarity of the graphical presentation symbols have been used in increments of approximately $\Delta T \approx 0.10$ in addition to solid lines. These numbers are adjusted in cases where a greater resolution of the phase diagrams is wanted.

B. Phase behavior without external field

In the absence of the external field and in the limit $x_2'' = 1.00$ our model system reduces to a pure Heisenberg fluid. Depending on the Heisenberg coupling parameter ε_H one anticipates three topologically distinct phase diagrams [8,13].

For weak coupling between the Heisenberg spins ($\varepsilon_H \lesssim 0.06$) one finds coxistence between a gas (G) and a polar (P) liquid phase ($\mathcal{P}_{l\geqslant 1} \neq 0$) at lower T, whereas at higher T a G phase coexists with an isotropic (I) (i.e., disordered) liquid phase. The junction between I and P phases, respectively, constitutes a critical end point at which a line of critical points starts that extends to higher T (see Fig. 1(a) of Ref. [13]). We refer to this as a "type I" phase diagram.

At intermediate values of ε_H one observes the topologically richest phase diagram. Again at lower T one has coexistence between G and P phases. As T increases, however, the phase diagram shows separate coexistence between the G and I and the I and P phases such that there is a narrow one-phase region of stable I phases. The critical line is shifted to higher T and starts at a tricritical point instead of a critical end point. A triple point exists at which the G, I, and P phases coexist (see Fig. 1(b) of Ref. [13]). Phase diagrams of this type have been termed "type II."

In the strong-coupling limit ($\varepsilon_H \gtrsim 0.11$) the GI critical point is suppressed such that a disordered fluid phase coexists with an ordered phase (see Fig. 1(c) of Ref. [13]). The isotropic fluid phase spans a rather broad density range. Phase diagrams of this general topology are referred to as "type III." These three types of phase diagrams seem generic. For example, they do not depend on the degree of sophistication of the mean-field approximation on which the DFT is based [13].

Focusing now on a suspension of magnetic particles in a solvent rather than a pure fluid containing only magnetic particles, we begin our discussion with the case of strong coupling between the Heisenberg spins. Specifically, we consider the case $\varepsilon_H = 0.12$ and $\varepsilon_{12} = 1.40$ such that a strong tendency to blend is realized for both mixture components.

If the concentration of magnetic particles is sufficiently low the phase diagram plotted in Fig. 1(a) reveals that on the liquid side only I phases exist. At these low concentrations the magnetic particles cannot organize themselves into an ordered phase, at least not over the temperature range numerically accessible. Both the G and the I phase boundaries in Fig. 1(a) merge at the mean-field critical point. Compared with a pure Heisenberg fluid the critical temperature T_c appears to be elevated by about 20% in the present case which is largely ascribed to the relatively strong attraction between a magnetic particle and a solvent molecule. This conclusion is drawn on the basis that in a pure Heisenberg fluid the spin-spin interaction is largely irrelevant for the location of the GI critical

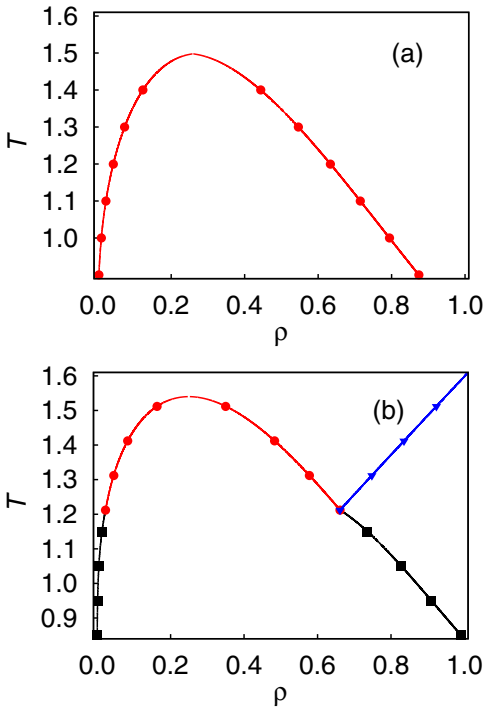

FIG. 1. (Color online) Phase diagrams in temperature T versus total number density ρ representation. Data have been obtained for $\varepsilon_H = 0.12$ and $\varepsilon_{12} = 1.40$. (a) $x_2'' = 0.25$, GI phase coexistence (—, ●) and (b) $x_2'' = 0.55$, GP (—, ■) and GI phase coexistence (—, ●). Also shown is the critical line (—, ▼) starting at a critical end point (see text).

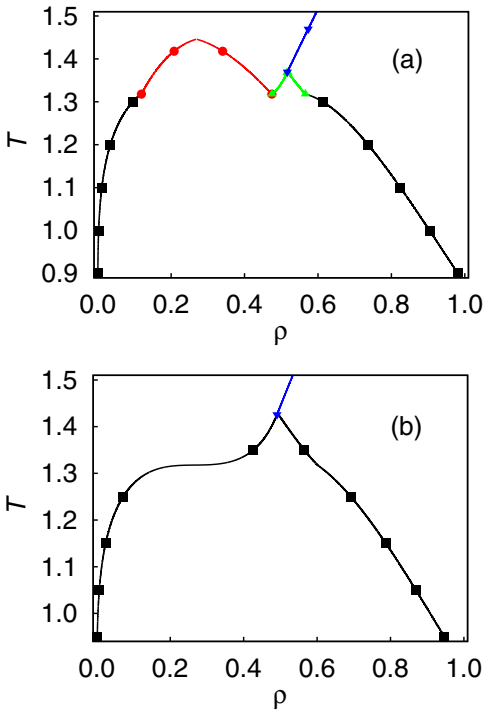

FIG. 2. (Color online) As Fig. 1 but for (a) $x_2'' = 0.85$ where one has GP (—, ■), GI (—, ●), and IP (—, ▲) phase coexistence; (b) $x_2'' = 0.95$ where a nonpolar fluid phase ($\rho \lesssim 0.50$) coexists with a P phase (—, ■). Also shown is the beginning of a critical line (—, ▼) starting at a tricritical point.

point (see Figs. 1(a) and 1(b) of Ref. [13]). We shall call phase diagrams of this particular topology "type 0," henceforth.

This conclusion makes sense in comparison with the phase diagram plotted for a higher concentration of magnetic particles in Fig. 1(b). At the higher concentration there is a larger number of interactions between unlike molecules and yet a lower configurational potential energy. Because of that one would anticipate an elevated T_c in the present case. A comparison of plots in Figs. 1(a) and 1(b) confirms the anticipated increase of T_c with x_2''.

However, this logic also implies that the largest T_c should be observed if the number of interactions between unlike molecules is maximum which is obviously the case for $N_1 = N_2 = N/2$. This notion is confirmed by the plot in Fig. 3 which shows that the GI critical temperature passes through a maximum at $x_2'' = 0.50$ and is symmetric with respect to that concentration as expected.

Another interesting feature is that, depending on the concentration of magnetic particles, all three generic phase diagrams described at the beginning of this section for pure Heisenberg fluids are recovered as plots in Figs. 1(b), 2(a), and 2(b) clearly show. The participation of ordered liquid phases in the phase diagrams of type I and II is illustrated by plots of the order parameter $\mathcal{P}_1$ along the liquid-phase boundary in Fig. 4. For the system at the lower concentration of magnetic particles $x_2'' = 0.55$ the plot of $\mathcal{P}_1$ drops to zero at the critical end point and stays at zero until the GI critical point at $T_c \simeq 1.520$ is reached. Similarly, the plot of $\mathcal{P}_1$ for $x_2'' = 0.85$ goes to zero at the tricritical temperature. In this latter case, notice a small dent in the plot of $\mathcal{P}_1$ versus T corresponding to the GIP triple point in Fig. 2(a).

This recovery of the three generic phase diagrams known for the pure Heisenberg fluid makes sense if one recalls that, in essence, in a mean-field treatment one considers the *overall* attractive field exerted on a reference molecule by its neighbors. Because in our model only the magnetic particles carry a spin, the overall attraction between a reference spin and its neighbors increases monotonically with the concentration of magnetic particles even though the Heisenberg coupling constant ε_H stays fixed. From this line of argument it is then

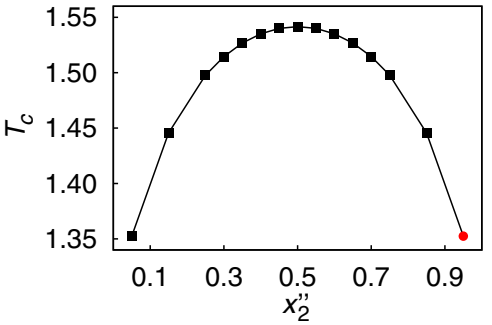

FIG. 3. (Color online) Variation of the gas- (isotropic) liquid critical temperature T_c with the concentration of magnetic particles in the liquid phase x_2''. Data have been obtained for $\varepsilon_H = 0.12$ and $\varepsilon_{12} = 1.40$. The point (●) does not correspond to a true critical point but rather represents the inflection point visible at about $\rho \simeq 0.25$ in Fig. 2(b).

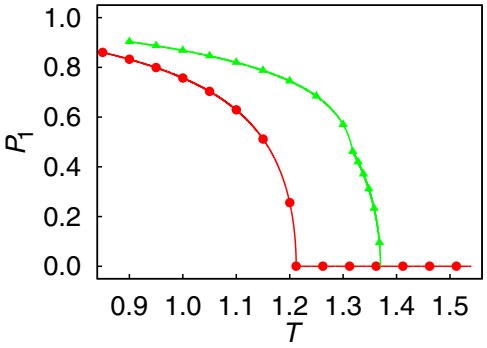

FIG. 4. (Color online) The order parameter $\mathcal{P}_1$ as a function of temperature T along the phase boundaries of P and I phases. Both curves have been obtained for $\varepsilon_H = 0.12$ and $\varepsilon_{12} = 1.40$ but for $x_2'' = 0.55$ (—, ●) [see Fig. 1(b)] and $x_2'' = 0.85$ (—, ▲) [see Fig. 2(a)].

to be expected that at constant ε_H types I–III phase diagrams are observed in our binary mixture with increasing x_2'' in very much the same fashion as these topologically distinct phase diagrams arise in a pure Heisenberg fluid with increasing ε_H.

The above phase diagrams have been obtained for a situation where blending of the two mixture components is energetically favored, that is, for $\varepsilon_{12} > 1.00$. For reasons of comparison, a typical phase diagram, where decomposition of the binary mixture is energetically favored, is shown in Fig. 5. The topology of the phase diagram is of type I as its counterpart depicted in Fig. 1(b). A comparison of Figs. 1(b) and 5 also reveals that T_c for $\varepsilon_{12} = 0.80$ is lowered substantially for reasons already explained.

However, the plot in Fig. 5 exhibits a peculiarity of the phase boundary of the G phase and temperatures up to the temperature of the critical end point. Compared with the previously discussed phase diagrams the curvature of the G-phase boundary differs. This different curvature, which seems unusual, may be a consequence of the constraint $x_2'' =$ const subject to which the phase diagram has been obtained. We have tested that this feature of the phase diagram is not an artifact by starting the minimization of Ω from different initial conditions without any appreciable effect on the final results. For temperatures above that of the critical end point the curvature of the phase boundary of the G phase becomes the same as for all other phase diagrams discussed so far. In

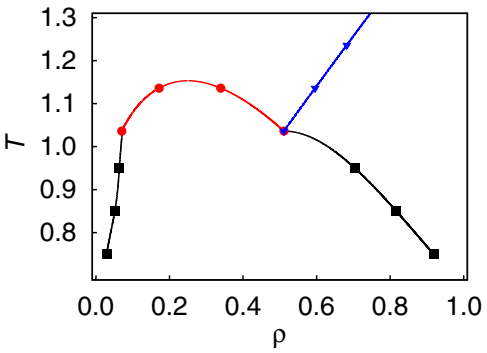

FIG. 5. (Color online) As Fig. 1(b) but for $\varepsilon_{12} = 0.80$.

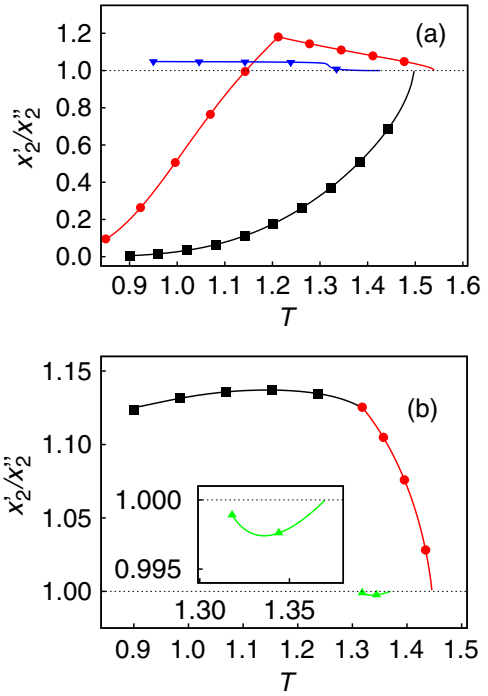

FIG. 6. (Color online) "Reduced" concentration of magnetic particles x_2'/x_2'' as functions of temperature T along the coexistence lines. (a) (—, ■) $x_2'' = 0.25$ [see Fig. 1(a)], (—, ●) $x_2'' = 0.55$ [see Fig. 1(b)], and (—, ▼) $x_2'' = 0.95$ [see Fig. 2(b)]; (b) as in part (a) but for $x_2'' = 0.85$ and GP (—, ■), GI (—, ●), and IP phase coexistence (—, ▲) [see Fig. 2(a)]. Solid lines in both parts of the figure are intended to guide the eye. In all cases $\varepsilon_H = 0.12$ and $\varepsilon_{12} = 1.40$.

other words, the G phase boundary seems to have an inflection point at the temperature of the critical end point.

Also shown in Figs. 1(b), 2(a), 2(b), and 5 is the line of critical points separating stable I from P phases. The critical lines are constructed through a Landau expansion as detailed elsewhere [8,13,16,22]. In the present case, where only magnetic particles are capable of being ordered, one obtains

$$\rho_{2c} = -\frac{2}{3}\frac{1}{u_1} \tag{4.3}$$

for the partial number density ρ_{2c} along the critical line. Because phase diagrams presented in this work are plotted in T–ρ representation at constant x_2'' the *total* density along the critical line is obtained from the relation $\rho_c = \rho_{2c}/x_2''$. This latter quantity is, in fact, the one plotted in Figs. 1(b), 2(a), 2(b), and 5. For phase diagrams of type I [see Figs. 1(b) and 5] the critical line terminates at a critical end point, whereas it ends in a tricritical point in phase diagrams of type II or III [8,13]. This is again a feature that is observed in phase diagrams for the pure Heisenberg fluid as the coupling strength of the spin-spin interaction increases [8,13].

An interesting aspect that takes the present binary pseudomixture beyond the realm of features that have already been observed for pure Heisenberg fluids concerns the variation of concentration in both phases $'$ and $''$. Plots of the "reduced" concentration x_2'/x_2'' along the coexistence curve in Fig. 6(a) reveal a rather complex variation of x_2'/x_2'' with T depending

on the (fixed) mole fraction x_2'' (i.e., the topology of the phase diagram).

For example, for $x_2'' = 0.25$ the corresponding plot in Fig. 6(a) shows that at the lowest T the G phase is pure and consists of solvent molecules only ($x_2' \simeq 0.00$). Their concentration decreases monotonically with increasing T (i.e., x_2' increases with T), that is, the G phase becomes more enriched with magnetic particles relative to the I phase the higher the T is. However, $x_2'/x_2'' \leqslant 1.00$ regardless of T where the equal sign applies at $T = T_c$. This is because at T_c, the G and I phases become indistinguishable.

At a higher concentration of magnetic particles $x_2'' = 0.55$ and starting from low T, x_2'/x_2'' increases monotonically at first. In other words, the G phase initially becomes richer in magnetic particles qualitatively similar to the previously discussed case. If T is sufficiently high, $x_2'/x_2'' > 1.00$ indicating that now the G phase is richer in magnetic particles than the P phase. The maximum of x_2'/x_2'' is reached at the critical end point. Beyond that point we have GI phase equilibrium [see Fig. 1(b)] and now x_2'/x_2'' decreases with increasing T, indicating that it is increasingly less favorable to have magnetic particles in the G phase relative to the I phase. This trend continues as $T \to T_c$; for $T = T_c$, $x_2'/x_2'' = 1.00$ for reasons already explained.

In the case $x_2'' = 0.95$, x_2'/x_2'' is approximately constant and slightly larger than one until one reaches a temperature $T \simeq 1.318$ at which the coexistence curve plotted in Fig. 2(b) reaches its plateau. For all larger T, $x_2'/x_2'' \simeq 1.00$ up to the temperature at the tricritical point where the coexistence curve in Fig. 2(b) terminates.

An interesting situation is encountered for $x_2'' = 0.85$ as the plot in Fig. 6(b) indicates. If $'$ is the G phase the concentration of magnetic particles in that phase is always larger than the one in either the P or I phases. With increasing T, x_2'/x_2'' first increases up to a temperature $T \simeq 1.146$; for larger T, x_2'/x_2'' declines monotonically towards the GI critical temperature at which x_2'/x_2'' again becomes unity.

Moreover, from the corresponding phase diagram in Fig. 2(a) it is clear that one also has IP phase coexistence between the triple point at $T_{\rm tr} \simeq 1.318$ and the tricritical point. In other words, one has phase equilibrium between two liquid phases, one disordered and the other one ordered. From the inset in Fig. 6(b) one sees that $x_2'/x_2'' < 1.00$, albeit the effect is small. Hence, magnetic particles prefer to stay in the ordered phase.

However, whether or not magnetic particles prefer to stay in the liquid phase depends crucially on whether an ordered liquid phase is available. For example, plots in Fig. 7(a) show that for very low concentrations $x_2'' = 0.05$ and low T almost all the magnetic particles prefer the G phase. As T increases x_2'/x_2'' decreases monotonically towards its limiting value of 1.00 at the GI critical point. Even though a few magnetic particles are present in the liquid phase, their concentration is too low to be able to form an ordered liquid phase as the corresponding plot of $\mathcal{P}_1$ in Fig. 7(b) clearly shows. If, on the contrary, the concentration of magnetic particles in the liquid phase is higher, the plot for $x_2'' = 0.55$ in Fig. 7(a) exhibits the opposite trend. Now only very few magnetic particles prefer the G phase at sufficiently low T because an ordered P phase coexists that accommodates magnetic particles conveniently. That an ordered phase forms for $x_2'' = 0.55$ is clear from

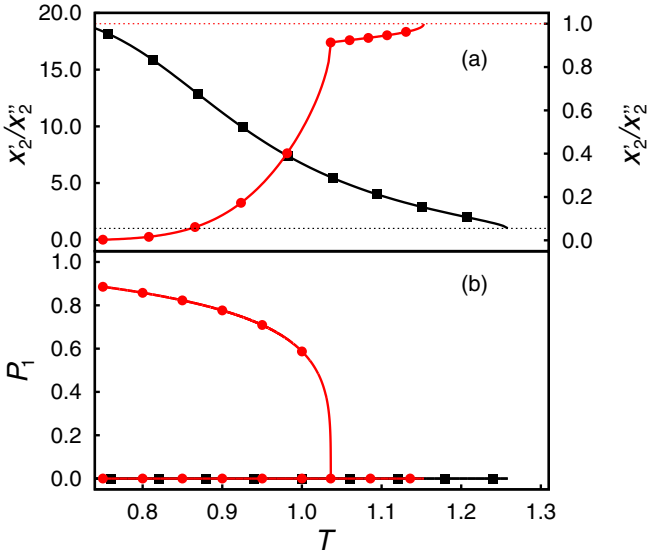

FIG. 7. (Color online) (a) As in Fig. 6 but for $x_2'' = 0.05$ (■, ——) (right ordinate) and $x_2'' = 0.55$ (●, ——) (left ordinate). (b) As in Fig. 4 but for the same "reduced" concentrations as in part (a) of the figure. In both parts data have been generated for $\varepsilon_{12} = 0.80$ and $\varepsilon_H = 0.12$.

the plot of the order parameter in Fig. 7(b). For this higher concentration of magnetic particles x_2'/x_2'' increases steadily with T up to T_c [see Fig. 7(a)]. Notice also in Fig. 7(a) that both sets of data show a strong tendency of the mixture to decompose at low T on account of our choice of $\varepsilon_{12} = 0.80$.

After having discussed details of the various types of phase diagrams it is perhaps instructive to get a broader overview of the types of phase diagrams that one anticipates for certain combinations of the model parameters ε_H, ε_{12}, and x_2''. Generally speaking, phase diagrams of type 0 (no participation of ordered phases) exist if the concentration of magnetic particles in phase $''$ is relatively low. These concentrations may be a bit higher if the solvent and the magnetic particles have a larger tendency to blend (i.e., for values of $\varepsilon_{12} > 1.00$; see Fig. 8).

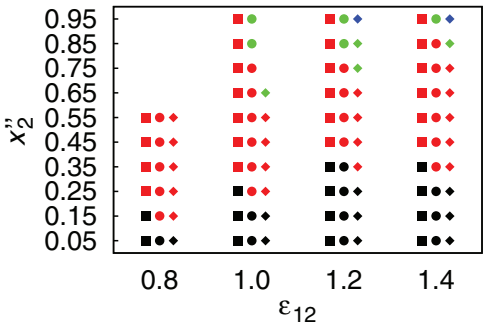

FIG. 8. (Color) Overview of types of phase diagrams encountered depending on the strength of spin-spin coupling ε_H, the strength of interaction between unlike molecules ε_{12}, and the mole fraction of magnetic particles in the denser phase x_2''. Squares: $\varepsilon_H = 0.06$; circles: $\varepsilon_H = 0.09$; diamonds: $\varepsilon_H = 0.12$. Color is used to identify specific types of phase diagrams. Black symbols: type 0; red symbols: type I; green symbols: type II; blue symbols: type III. In regions in which symbols are missing no stable solutions of Eqs. (4.1) and (4.2) could be obtained.

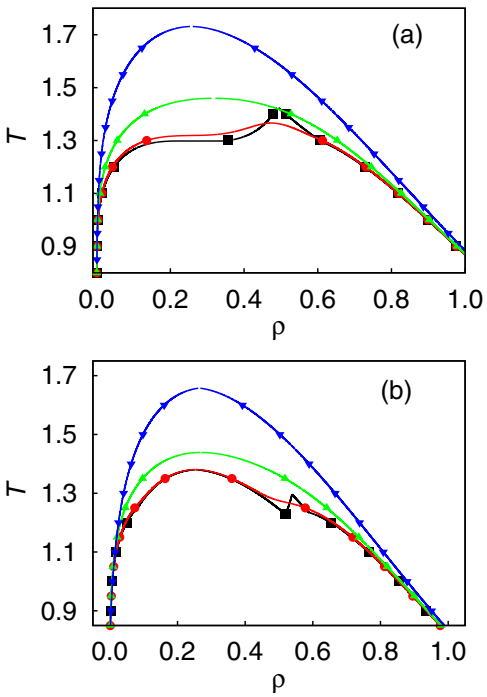

FIG. 9. (Color online) As in Fig. 1 but for $\varepsilon_H = 0.12$, $\varepsilon_{12} = 1.20$, and $H = 0.00$ (■, ——), $H = 0.10$ (●, ——), $H = 1.00$ (▲, ——), and $H = 10.00$ (▼, ——); (a) $x_2'' = 0.95$, (b) $x_2'' = 0.75$. For data sets corresponding to $H = 0.00$ critical lines have been omitted for the sake of clarity of the plots in both parts of the figure.

The scheme in Fig. 8 turns out to be dominated by phase diagrams of type I which appear to be stable for a broad range of mole fractions x_2'', strength of spin-spin coupling ε_H, and interaction strength between unlike molecules ε_{12}.

Compared with phase diagrams of type I, those of type II are much more restricted to areas in parameter space in which ε_H is sufficiently high but also x_2'' is large as well. Phase diagrams of type II are observed only if the two components do not demix.

Last but not least, phase diagrams of type III are only rarely observed. They are restricted to the highest concentrations, spin-spin coupling strengths, and mixtures in which the two components exhibit a strong tendency to blend.

C. Phase behavior for nonvanishing external fields

Next we turn to a discussion of the impact of the external homogeneous magnetic field on the phase behavior of the suspension of magnetic particles in a nonmagnetic solvent. Because of the relatively high dimension of the parameter space of our model system we restrict the discussion to those cases that turned out to be the most interesting ones. Thus, we concentrate on phase diagrams that are of types II and III in the absence of the external field. As we showed in Sec. IV B these topologies are obtained at relatively high concentrations of magnetic particles x_2'' in the liquid phase. Intuitively, one would expect these suspensions to be most sensitive to the presence and strengths of the external field because the binary mixture contains enough particles to respond to such a field.

We begin our presentation of results in Fig. 9(a) with a phase diagram that is of type III in the absence of the external field. For this topology the concentration of magnetic particles in the liquid phase is sufficiently large so a GI critical point is suppressed. However, there is a tricritical point clearly visible in the phase diagram where the phase boundary between a high-density, isotropic fluid phase and a P phase join.

TABLE I. Critical temperature T_c and density ρ_c for various concentrations of magnetic particles x_2'' and different external magnetic fields H.

H	x_2''	T_c	ρ_c	Phase diagram
1.00	0.75	1.439	0.267	Type II
10.00	0.75	1.657	0.261	Type II
1.00	0.95	1.450	0.312	Type III
10.00	0.95	1.731	0.253	Type III

As soon as H is nonzero, the tricritical point vanishes. This is true even for infinitesimally small H. However, a vestige of the former tricritical point remains as one can see by comparing in Fig. 9(a) plots for $H = 0.00$ and $H = 0.10$. The triangular-shaped region around the tricritical point visible in the plot for $H = 0.00$ has given way to a rather broad maximum in the phase diagram for $H = 0.10$.

For larger external fields even that broad maximum eventually disappears as one can see in Fig. 9(a) from the plots for $H = 1.00$ and $H = 10.00$. Instead, a GI critical point reappears. The higher the H the more elevated is the critical temperature T_c. At the same time, the critical density ρ_c turns out to be shifted to lower values as one can clearly see in Fig. 9(a).

A much smaller shift is observed upon varying ε_H in a pure fluid composed of only magnetic particles [13]. On the contrary, the shift of the critical density in the present case is fairly pronounced as entries in Table I indicate. Hence, as H increases there is a topological change in the phase diagram from type III in the absence of an external field to something reminiscent of a type 0 topology in the presence of such an external field.

Comparing plots in Fig. 9(a) with those in Fig. 9(b) one notices qualitatively similar features as H varies. However, here we are confronted with a phase diagram of type II in the absence of the external field. These phase diagrams have a GI critical point. Phase coexistence between I and P phases terminates again at a tricritical point at the end of the tiny triangular shaped region in the plot for $H = 0.00$ in Fig. 9(b).

Again, any nonzero external potential suppresses tricriticality (and with it the critical line) [see, for example, Fig. 2(a)]. In fact, as one sees from the plot for $H = 0.10$ in Fig. 9(b), IP phase coexistence has disappeared and has left as its remnant the broad shoulder visible at densities slightly below 0.60. This shoulder vanishes at higher external potentials $H = 1.00$ and $H = 10.00$ similar to the disappearance of the broad maximum in the curve for $H = 0.10$ in Fig. 9(a).

A comparison of plots in Fig. 9(a) with their counterparts in Fig. 9(b) reveal that the two phase region is wider at the higher concentration of magnetic particles x_2''. At the same time the upward shift of the critical temperature T_c with H, on the one hand, is somewhat more substantial for $x_2'' = 0.95$ compared with $x_2'' = 0.75$ as respective entries in Table I indicate. The shift to lower critical densities ρ_c observed for $x_2'' = 0.95$, on the other hand, is negligibly small for $x_2'' = 0.75$.

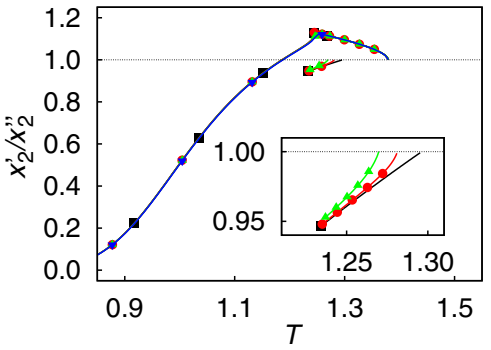

FIG. 10. (Color online) As in Fig. 6 but for $H = 0.000$ (■, ——), $H = 0.001$ (●, ——), $H = 0.005$ (▲, ——), and $H = 0.010$ (▼, ——). For all curves $\varepsilon_H = 0.12$, $\varepsilon_{12} = 1.20$, and $x_2'' = 0.75$ [cf. Fig. 9(b)]. Inset: An enhancement showing only the short branch corresponding to IP phase coexistence (see text).

Plots in both parts of Fig. 9 reveal that the most pronounced impact of the external field on the phase behavior occurs for small H. As far as the corresponding composition of phases $'$ and $''$ is concerned we notice from Fig. 10 that the plots consist of two branches, a longer one where $'$ is the G phase and a much shorter one along where $'$ is the I phase and $x'/x'' \leqslant 1.00$ [Fig. 9(b)]. For the longer branch apparently the weak external field is largely irrelevant.

For the shorter branch the inset in Fig. 10 exhibits two features. In agreement with Fig. 9(b) the short branch vanishes somewhere in the range $0.005 < H < 0.010$. Over the range $0.000 \leqslant H \leqslant 0.005$ the tricritical temperature (i.e., the locus of $x_2'/x_2'' = 1.00$) shifts monotonically to smaller values with increasing H. At the same time the I phase becomes slightly more enriched with magnetic particles (i.e., x_2'/x_2'' increases), which is particularly noteworthy by comparing plots for $H = 0.001$ and $H = 0.005$ for the same T.

It is also instructive to amend the analysis of phase diagrams in Fig. 9 by plots of the order parameter $\mathcal{P}_1$ along the coexistence curve in Fig. 11. Starting again with the higher concentration of magnetic particles $x_2'' = 0.95$ in the absence of an external fields in Fig. 11(a) one notices that, beginning with states of large $\mathcal{P}_1$ and low T (P phase), the order parameter declines continuously until it vanishes at the tricritical point visible in the corresponding plot in Fig. 9(a). As T is then reduced again along the phase boundary of the I phase, $\mathcal{P}_1 = 0$ irrespective of T as it should.

If one increases the external field to $H = 0.10$ the plot of $\mathcal{P}_1$ turns out to be nearly indistinguishable from the one for $H = 0.00$. Both curves begin to deviate from each other for $\mathcal{P}_1 \lesssim 0.60$. For $H = 0.10$ the curve in Fig. 11(a) decays with an eventually positive slope until it assumes a small value in the range of $0.03 \lesssim \mathcal{P}_1 \lesssim 0.04$. Hence, no matter how small H is, only more or less ordered states exist along the coexistence curve.

Order of states in the lower-density phase increases markedly with H as Fig. 11(a) reveals for $H = 1.00$ and $H = 10.00$. In both curves $\mathcal{P}_1$ first decreases with increasing T until the critical point is reached [see Fig. 9(a)]. On the low-density side of the corresponding phase diagrams $\mathcal{P}_1$ eventually increases again with decreasing T as the magnetic

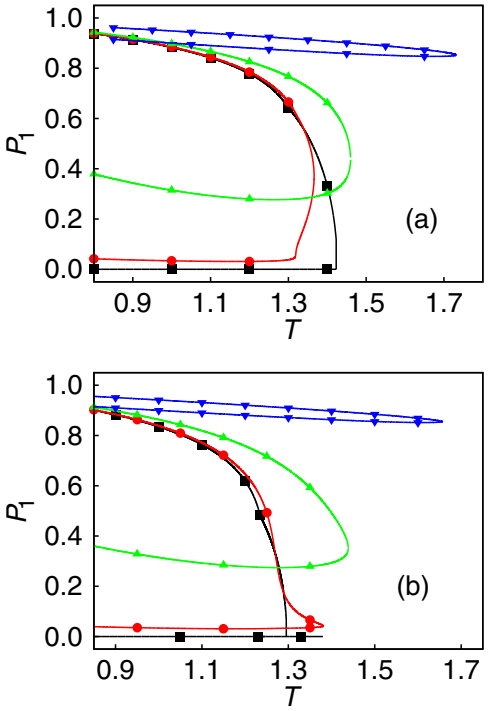

FIG. 11. (Color online) Variation of the order parameter $\mathcal{P}_1$ with temperature T along the entire coexistence curve and for $\varepsilon_H = 0.12$, $\varepsilon_{12} = 1.20$, and $H = 0.00$ (■, ——), $H = 0.10$ (●, ——), $H = 1.00$ (▲, ——), and $H = 10.00$ (▼, ——); (a) $x_2'' = 0.95$, (b) $x_2'' = 0.75$.

particles are losing thermal energy. Notice also from Fig. 11(a) that for a sufficiently high external field $H = 10.00$, $\mathcal{P}_1$ along the low-density phase boundary stays almost as high as $\mathcal{P}_1$ along its high-density counterpart.

Comparing plots in Fig. 11(a) with those in Fig. 11(b) reveals only rather subtle differences. For example, $\mathcal{P}_1$ for $H = 0.00$ drops to zero with increasing T at the tricritical point as before. However, because the phase diagram exhibits a GI critical point in Fig. 9(b) that part of the corresponding plot in Fig. 11(b) characterized by $\mathcal{P}_1 = 0$ ends at T_c, which slightly exceeds the temperature at the tricritical point [see Fig. 9(b)].

V. DISCUSSION AND CONCLUSIONS

In this work we apply DFT to suspensions of magnetic particles in a nonmagnetic solvent where the former carry a classical, three-dimensional spin that allows them to interact with an external magnetic field. The solvent is composed of spherically symmetric Lennard-Jones-type molecules that have no orientational degrees of freedom. In the absence of an external field, the only relevant parameters are the interaction strength between unlike particles ε_{12} and the spin-spin coupling constant ε_H.

As far as the thermodynamic state is concerned and because we explicitly assume phase coexistence, the grand potential Ω depends *explicitly* only on temperature T and *implicitly* on the external field H as the only two thermodynamic parameters. The implicit dependence on H arises via the orientation distribution function $\alpha(\omega)$.

From a numerical perspective and from a somewhat naive point of view, we are confronted with a situation where we have to solve a set of five coupled nonlinear equations for six variables. Seemingly, this poses a problem in that a unique solution cannot be obtained. However, this ostensible problem can be circumvented by realizing that if one fixes the concentration of one of the two components in either of the two phases a sixth equation naturally links the partial number densities of the two components in that phase. Therefore, our numerical problem is no longer underdetermined.

We have deliberately chosen the mole fraction of the magnetic particles in the liquid phase x_2'' as this new thermodynamic state parameter (besides T and H). Indeed, from an experimental perspective it seems easier to control the net weight of both components in the liquid phase ($x_1'' + x_2'' = 1$) rather than that in the gas phase.

Depending on choices of model and thermodynamic state parameters rather complex phase behavior is observed. It turns out that four generic types of phase diagrams exist depending on the amount of magnetic particles present in the liquid phase at fixed coupling strength ε_H of the spin-spin interaction. In a pure fluid composed of the same magnetic particles the same four generic phase diagram topologies are observed [8,13].

To explain this similarity we argue that, at mean-field level, it is only the *net* attraction of the spin-spin coupling that matters for the formation of ordered phases. This net attraction is determined by the concentration of the magnetic particles in the present two-component suspension or the coupling strength itself in the case of a pure fluid of such particles. Whereas this result may have been anticipated from the very beginning, it is nonetheless gratifying that it is indeed observed here because it validates our current approach of making x_2'' one of the input variables.

More interesting and not predictable from the outset is the variation of the concentration of magnetic particles in the lower-density phase relative to that in the higher-density one. Perhaps most notable in this regard is that one may observe liquid-liquid phase coexistence between isotropic and polar liquid phases. Here one of the phases is rich in magnetic particles and the other one turns out to be rich in solvent molecules. Solvent molecules prefer the I phase, whereas the presence of magnetic particles is enhanced in the P phase. However, the effect is admittedly small because the length of the phase boundaries separating isotropic from polar liquids is tiny in the current model suspension. This could be quite different if the current magnetic compound would be replaced by a liquid crystal phase [44].

For liquid crystals one of the simplest phase equilibria between liquidlike phases is that between an isotropic and a nematic liquid. For the model used in an earlier study [44] it was found that for temperatures slightly above that of a triple point, at which a gaseous phase coexists simultaneously with an isotropic and a nematic liquid phase, the density difference between coexisting isotropic and nematic phases is much more pronounced than that characteristic of coexisting I and P phases in the current model. Hence, if the liquid crystal is dissolved in a solvent similar to the one used here it might be conceivable that a more pronounced difference in concentration of both mixture compounds in the coexisting liquidlike phases arises.

As far as a nonvanishing external magnetic field is concerned, the effects are threefold. First, the critical line separating isotropic from polar phases is completely suppressed for any nonvanishing H. Second, for any nonvanishing H one always observes coexistence between phases that are always ordered to a certain degree. The one at lower density is usually less ordered than the one at higher density. This difference in the degree of order along the coexistence curve diminishes as H becomes larger. At intermediate H one may have situations in which order decreases monotonically along the phase boundary of the higher-density phase as T increases towards the gas-liquid critical point. At the same time, the degree of order in the low-density phase behaves nonmonotonically with T. Third, at sufficiently low H details of the dependence of order on T are determined by the type of phase diagram that one is confronted with in the limit of vanishing H.

In summary, our study reveals that mixtures of Heisenberg spheres, which may be considered as elementary models for magnetic particles, and neutral spheres (representing a solvent) display a rich phase behavior, which is moreover tunable by an external field. Our results complete earlier theoretical and computer simulation investigations of pure Heisenberg fluids, as well as studies of mixtures of other (i.e., Ising, XY) spin fluids. Comparing the phase behaviors of the Heisenberg mixtures obtained in our present study with those in dipolar mixtures, one finds that the general topologies of the phase diagrams are similar (see, for example, Refs. [23,24]). However, there are also differences, an example being the dependence of the critical demixing temperature on an external field. While in the Heisenberg case, this temperature just increases with H (due to the above mean-field argument targeting the increase of attraction), dipolar mixtures reveal a nonmonotonic dependence [25] reflecting the more complicated character of the interaction which disfavors side-by-side configurations of parallel dipoles. Clearly, such features may become important if one attempts to model real mixtures involving ferromagnetic (nano-) particles at high densities. However, as stated initially, one main advantage of the classical Heisenberg model is that, at least in the one-component case, MMF-DFT calculations are quite accurate. Naturally, it would be very important to do the same test for the present theoretical results. We therefore hope that our results stimulate future simulations.

ACKNOWLEDGMENTS

We are grateful to Deutsche Forschungsgemeinschaft (DFG) for financial support under the auspices of the International Graduate Research Training Group (IRTG) 1524 "Self-assembled soft matter nanostructures at interfaces." In addition, S.H.L.K. acknowledges DFG for support via the Priority Programme SPP 1681 "Field controlled particle matrix interactions: synthesis multiscale modeling and application of magnetic hybrid materials."

APPENDIX: NONLINEAR EQUATIONS DESCRIBING COEXISTING PHASES AT THERMODYNAMIC EQUILIBRIUM

Here we summarize the equations that we need to solve numerically to determine the phase boundary separating coexisting phases $'$ and $''$. At coexistence and at fixed T the

associated pressures P' and P'' have to be the same. From Eq. (3.24) pressure equality in the two phases corresponds to

$$s_1 = -\rho' + \rho'' + \rho'\frac{2\eta' - 4\eta'}{(1-\eta')^3} - \rho''\frac{2\eta'' - 4\eta''}{(1-\eta'')^3} - \frac{u_0}{4}\left(\rho_1'^2 - \rho_1''^2\right) - \frac{u_0}{4}\left(\rho_2'^2 - \rho_2''^2\right) - \frac{u_0^{(12)}}{2}\left(\rho_1'\rho_2' - \rho_1''\rho_2''\right) - u_1\left(\rho_2'^2\alpha_1'^2 - \rho_2''^2\alpha_1''^2\right) = 0. \tag{A1}$$

Similarly, the conditions for minima of the grand potential Eqs. (3.20) and (3.23) allow one to introduce the functions

$$s_2 = \ln\left(\frac{\rho_1'}{\rho_1''}\right) + \frac{8\eta' - 9\eta'^2 + 3\eta'^3}{(1-\eta')^3} - \frac{8\eta'' - 9\eta''^2 + 3\eta''^3}{(1-\eta'')^3} + \frac{u_0}{2}(\rho_1' - \rho_1'') + \frac{u_0}{2}(\rho_2' - \rho_2'') = 0 \tag{A2}$$

and

$$s_3 = \ln\left(\frac{\rho_2'}{\rho_2''}\right) + \frac{8\eta' - 9\eta'^2 + 3\eta'^3}{(1-\eta')^3} - \frac{8\eta'' - 9\eta''^2 + 3\eta''^3}{(1-\eta'')^3} + \frac{u_0}{2}(\rho_2' - \rho_2'') + \frac{u_0^{(12)}}{2}(\rho_1' - \rho_1'') - \ln\frac{\sinh(a')}{a'} + \ln\frac{\sinh(a'')}{a''} = 0, \tag{A3}$$

where $a'^{,''} \equiv 9\rho_2'^{,''}u_1\mathcal{P}_1'^{,''}/2 - \beta H$. Notice that in writing Eqs. (A2) and (A3) we have again been assuming equilibrium conditions, that is, $\mu_i' = \mu_i''$ $(i = 1,2)$. From Eq. (3.25) two more equations can be derived, namely

$$s_{4,5} = \alpha_1'^{,''} - \frac{3}{2}\frac{\tanh(a'^{,''}) - a'^{,''}}{a'^{,''}\tanh(a'^{,''})} = 0 \tag{A4}$$

for the order parameters of the magnetic particles in the gas and in the liquid phase, respectively (see also Appendix B of Ref. [13]). So far we established five equations for six unknowns identified at the end of Sec. III. However, a sixth such equation may be introduced by realizing that for a given input mole fraction of the magnetic particles x_2''

$$s_6 = \frac{x_2''}{1 - x_2''}\rho_1'' - \rho_2'' = 0, \tag{A5}$$

which follows directly from the definition of the mole fraction of the magnetic particles in the liquid phase.

[1] P. C. Hemmer and D. Imbro, Phys. Rev. A **16**, 380 (1977).
[2] I. P. Omelyan, W. Fenz, I. M. Mryglod, and R. Folk, Phys. Rev. Lett. **94**, 045701 (2005).
[3] I. P. Omelyan, I. M. Mryglod, R. Folk, and W. Fenz, Phys. Rev. E **69**, 061506 (2004).
[4] I. P. Omelyan, R. Folk, A. Kovalenko, W. Fenz, and I. M. Mryglod, Phys. Rev. E **79**, 011123 (2009).
[5] E. Lomba, J. J. Weis, and C. F. Tejero, Phys. Rev. E **58**, 3426 (1998).
[6] E. Lomba, J. J. Weis, N. G. Almarza, F. Bresme, and G. Stell, Phys. Rev. E **49**, 5169 (1994).
[7] F. Lado, E. Lomba, and J. J. Weis, Phys. Rev. E **58**, 3478 (1998).
[8] J. M. Tavares, M. M. Telo da Gama, P. I. C. Teixeira, J. J. Weis, and M. J. P. Nijmeijer, Phys. Rev. E **52**, 1915 (1995).
[9] A. Oukouiss and M. Baus, Phys. Rev. E **55**, 7242 (1997).
[10] K. Moon and S. M. Girvin, Phys. Rev. Lett. **75**, 1328 (1995).
[11] T. Erdmann, M. Kröger, and S. Hess, Phys. Rev. E **67**, 041209 (2003).
[12] S. Giura, B. G. Márkus, S. H. L. Klapp, and M. Schoen, Phys. Rev. E **87**, 012313 (2013).
[13] M. Schoen, S. Giura, and S. H. L. Klapp, Phys. Rev. E **89**, 012310 (2014).
[14] D. Wei and G. N. Patey, Phys. Rev. Lett. **68**, 2043 (1992).
[15] L. Rovigatti, J. Russo, and F. Sciortino, Soft Matter **8**, 6310 (2012).
[16] B. Groh and S. Dietrich, Phys. Rev. E **50**, 3814 (1994).
[17] S. Klapp and F. Forstmann, J. Chem. Phys. **106**, 9742 (1997).
[18] R. Weeber, M. Klingikt, S. Kantorovich, and C. Holm, J. Chem. Phys. **139**, 214901 (2013).
[19] H. Schmidle, S. Jäger, C. K. Hall, O. D. Velev, and S. H. L. Klapp, Soft Matter **9**, 2518 (2013).
[20] S. Klapp and F. Forstmann, Europhys. Lett. **38**, 663 (1997).
[21] W. Fenz and R. Folk, Phys. Rev. E **71**, 046104 (2005).
[22] G. M. Range and S. H. L. Klapp, Phys. Rev. E **69**, 041201 (2004).
[23] G. M. Range and S. H. L. Klapp, Phys. Rev. E **70**, 031201 (2004).
[24] G. M. Range and S. H. L. Klapp, Phys. Rev. E **70**, 061407 (2004).
[25] G. M. Range and S. H. L. Klapp, J. Chem. Phys. **122**, 224902 (2005).
[26] I. Szalai and S. Dietrich, Mol. Phys. **103**, 2873 (2005).
[27] E. Diaz-Herrera and F. Forstmann, J. Chem. Phys. **102**, 9005 (1995).
[28] C. Brunet, J. G. Malherbe, and S. Amokrane, Mol. Phys. **110**, 1161 (2012).
[29] N. G. Almarza, E. Lomba, E. Martin, and A. Gallardo, J. Chem. Phys. **129**, 234504 (2008).
[30] J. S. Rowlinson and F. Swinton, *Liquids and Liquid Mixtures*, 3rd ed. (Butterworths, London, 1982).
[31] C. Hertlein, L. Helden, A. Gambassi, S. Dietrich, and C. Bechinger, Nature **451**, 172 (2008).
[32] A. J. Archer and R. Evans, J. Chem. Phys. **121**, 4246 (2004).
[33] K. Lichtner and S. H. L. Klapp, J. Chem. Phys. **136**, 024502 (2012).

[34] K. Lichtner and S. H. L. Klapp, Phys. Rev. E **88**, 032301 (2013).
[35] A. Malijevsky and A. J. Archer, J. Chem. Phys. **139**, 144901 (2013).
[36] K. Lichtner and S. H. L. Klapp, Europhys. Lett. **106**, 56004 (2014).
[37] R. Rungsawang, J. da Silva, C.-P. Wu, E. Sivaniah, A. Ionescu, C. H. W. Barnes, and N. J. Darton, Phys. Rev. Lett. **104**, 255703 (2010).
[38] P. Frodl and S. Dietrich, Phys. Rev. A **45**, 7330 (1992).
[39] G. Ayton, M. J. P. Gingras, and G. N. Patey, Phys. Rev. Lett. **75**, 2360 (1995).
[40] C. G. Gray and K. E. Gubbins, *Theory of Molecular Fluids*, Vol. 1 (Clarendon Press, Oxford, 1984).
[41] P. I. Teixeira and M. M. Telo da Gama, J. Phys.: Condens. Matter **3**, 111 (1991).
[42] M. Gramzow and S. H. L. Klapp, Phys. Rev. E **75**, 011605 (2007).
[43] N. F. Carnahan and K. E. Starling, J. Chem. Phys. **51**, 635 (1969).
[44] S. Giura and M. Schoen, Phys. Rev. E **90**, 022507 (2014).